



# Characterization of fuel gases with fiber-enhanced Raman spectroscopy

Anne Sieburg<sup>1</sup> · Andreas Knebl<sup>1,2</sup> · Jikku M. Jacob<sup>1</sup> · Torsten Frosch<sup>1,3,4</sup> 

Received: 17 May 2019 / Revised: 19 August 2019 / Accepted: 6 September 2019 / Published online: 16 September 2019  
© Springer-Verlag GmbH Germany, part of Springer Nature 2019

## Abstract

Common gaseous fuels are mixtures of several components. As the properties of the fuels can vary with the composition, but combustion needs to be stable, reliable analytical methods are highly sought after. Raman spectroscopic methods have proved their suitability for the characterization of diverse gaseous mixtures. They have the potential to overcome existing limitations of established technologies, since they are fast, non-consumptive, and accurate. Here, we demonstrate a gas sensor based on fiber-enhanced Raman spectroscopy (FERS) for fuel gas monitoring. Online detection of all gas components, including alkanes, carbon dioxide (CO<sub>2</sub>), nitrogen (N<sub>2</sub>), and hydrogen sulfide (H<sub>2</sub>S), for varying concentration ranges from tens of vol% down to the ppm level enables a comprehensive characterization of the fuels. The developed sensor system features a pinhole assembly which sufficiently reduces the background signal from the fiber to enable the detection of C<sub>2</sub>–C<sub>4</sub> alkanes occurring in low concentrations. Detection limits in the low ppm region were achieved for the minor components of fuel gases, which allow the online monitoring of necessary purification steps, e.g., for biogas. The obtained results indicate that fiber-enhanced Raman sensors have the potential for comprehensive online and onsite gas sensing for fuel gas quality control.

**Keywords** Raman spectroscopy · Fiber sensor · Hollow core photonic crystal fiber · Fuel gas · Sensing · Natural gas · Biogas

## Introduction

In recent years, the use of alternative fuels as energy source received renewed attention because the use of petroleum-

based fuels is rapidly depleting the natural reserves and increases the emission of greenhouse gases. Fuel gases have become a suitable and attractive alternative to petroleum-based fuel, caused by their versatility of use, for example, in gas engines, for heating, cooking, and electricity generation. Fuel gases can be classified depending on their source and the way of production [11]: naturally found fuel gases like natural gas or shale gas, and fuel gases produced from other materials like biogas. Many fuel gases are composed of hydrocarbons like methane (CH<sub>4</sub>), ethane (C<sub>2</sub>H<sub>6</sub>), or propane (C<sub>3</sub>H<sub>8</sub>) as well as other gases like carbon dioxide (CO<sub>2</sub>), or mixtures thereof. However, the composition and properties of these mixtures can vary significantly depending on the region where they are formed. The most common types of fuel gases in current use are natural gas [39] or biofuels like biogas [42].

To use biogas as fuel gas, gas pre-processing is necessary to enhance the CH<sub>4</sub> content and to reduce incombustible components like CO<sub>2</sub> or toxic and corrosive constituents like hydrogen sulfide (H<sub>2</sub>S) [2]. Additionally, an adaption to the gas quality of the natural gas in the gas grid is needed (Fig. 1). To ensure a compatible quality of gas, different process parameters are used to characterize fuel gases: the so-called Wobbe Index [61], which describes the interchangeability of gases, or

---

Published in the topical collection *Young Investigators in (Bio-)Analytical Chemistry* with guest editors Erin Baker, Kerstin Leopold, Francesco Ricci, and Wei Wang.

---

**Electronic supplementary material** The online version of this article (<https://doi.org/10.1007/s00216-019-02145-x>) contains supplementary material, which is available to authorized users.

---

✉ Torsten Frosch  
torsten.frosch@uni-jena.de; torsten.frosch@gmx.de

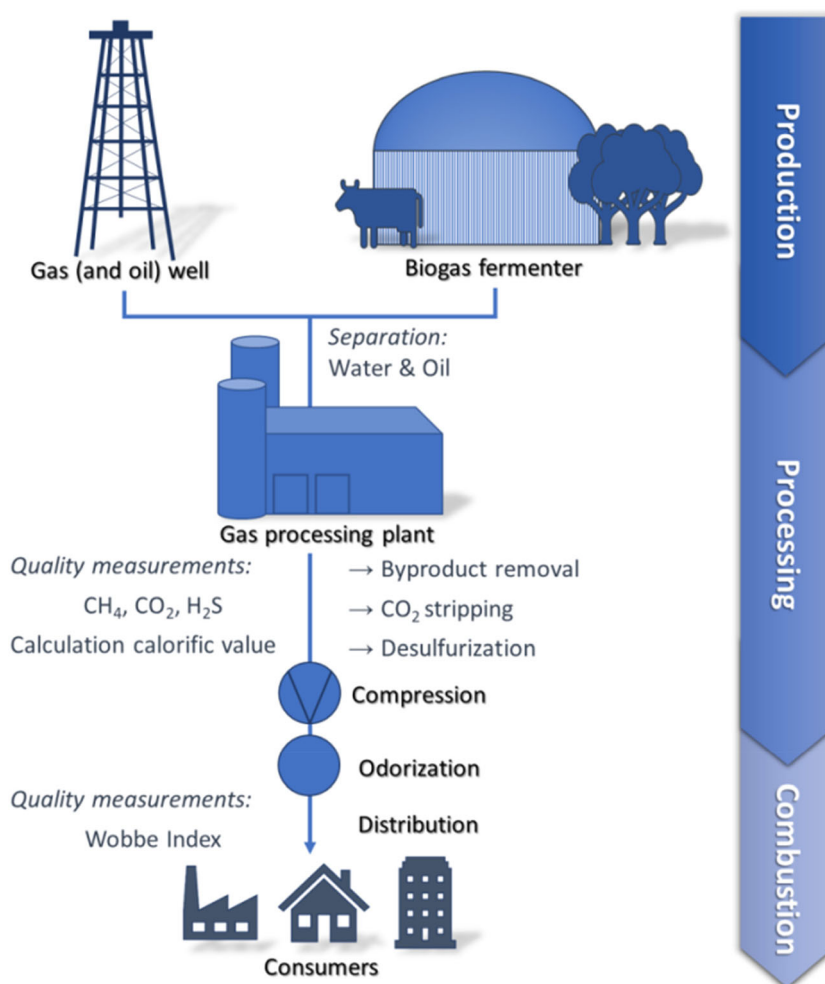
<sup>1</sup> Leibniz Institute of Photonic Technology, Albert-Einstein-Str. 9, 07745 Jena, Germany

<sup>2</sup> Max Planck Institute for Biogeochemistry, Beutenberg Campus, Hans-Knöll-Str. 10, 07745 Jena, Germany

<sup>3</sup> Institute of Physical Chemistry, Friedrich Schiller University, Lessingstr. 10, 07743 Jena, Germany

<sup>4</sup> Abbe Center of Photonics, Friedrich Schiller University, Albert-Einstein-Str. 6, 07745 Jena, Germany

**Fig. 1** Process chain and necessary quality measurements of fuel gases from production until combustion. Before biogas can be fed into the natural gas grid, the methane content must be increased, and carbon dioxide must be removed. Wobbe Index and the calorific value of a gas are important parameters for the interchangeability of fuel gases and must therefore be determined, before the fuel gas arrives at the consumer



the calorific value. The calorific value and hence the energy content strongly depend on the composition of the gas mixture [35]. Since the performance of the combustion-based energy conversion will change with changing fuel properties, suitable control strategies are required to avoid additional costs for the operators of such devices [3]. There are also a number of industrial processes, especially in glass, ceramics, or metal manufacturing, which may be significantly affected by local gas quality fluctuations [35]. Thus, analytical technologies capable of characterizing these fuel gases are highly sought after.

A variety of analytical methods can be used to describe a fuel gas representing a mixture of multiple components. The calorific value, for example, can be determined as single parameter using a calorimeter [53]. For other purposes, where a detailed compositional analysis is required, gas chromatography coupled with mass spectrometry (GC/MS) is the state of the art [52]. However, chromatography-based methods normally require sampling, and they are time-consuming and relatively expensive in terms of investment and operational costs. To overcome these restrictions, spectroscopic methods

have found more and more applications for the analysis of fuel gases in recent years [17, 31]. In particular, vibrational spectroscopic techniques like infrared absorption (IR) and Raman spectroscopy appear attractive as they are specific [5, 6, 13–15, 37], fast, and can be applied onsite and online. Nevertheless, currently established IR absorption-based sensors are limited in terms of measuring the homonuclear diatomic molecules hydrogen ( $H_2$ ) and nitrogen ( $N_2$ ). However, these are important for the characterization of fuel gases and can be detected with Raman spectroscopic devices [10, 32]. Raman spectroscopy is based on inelastic light scattering and can thus probe all but noble gases with only one laser light source. It has a number of advantages, including good sensitivity in a wide concentration range, fast measurements within seconds, as well as label-free and non-consumptive operation [8, 9, 38, 43, 46]. Novel enhancement techniques like cavity-enhanced Raman spectroscopy (CERS) [12, 29, 36, 44] or fiber-enhanced Raman spectroscopy (FERS) [18, 33, 34, 57] allow the investigation of low-concentrated analytes and show high potential in environmental [19, 25, 26, 28, 30, 50], therapeutic [4, 20, 47, 56, 58–60],

and process analysis [23, 24, 27, 41, 45, 51]. A very promising approach is FERS, which is based on the use of hollow core photonic crystal fibers (HC-PCF). Here, laser light is focused into and guided within the core of the sample filled fiber. This greatly increases the interaction between laser light and analytes, enhancing Raman signal generation. Additionally, the fiber also collects and guides the Raman scattered light. Overall, signal yield is greatly improved in FERS compared with common methods (up to three orders of magnitude lower detection limits can be achieved, e.g., 0.2 ppm instead of 200 ppm) [33].

In this paper, the application of a novel sensor based on fiber-enhanced Raman spectroscopy for the analysis of different fuel gases is demonstrated. This very sensitive and chemically selective technique was evaluated for process-relevant concentrations of important fuel gases. Since all relevant components can be detected simultaneously, the sensor is suitable for online monitoring of fuel gases, including H<sub>2</sub>S, CO<sub>2</sub>, N<sub>2</sub>, and alkanes.

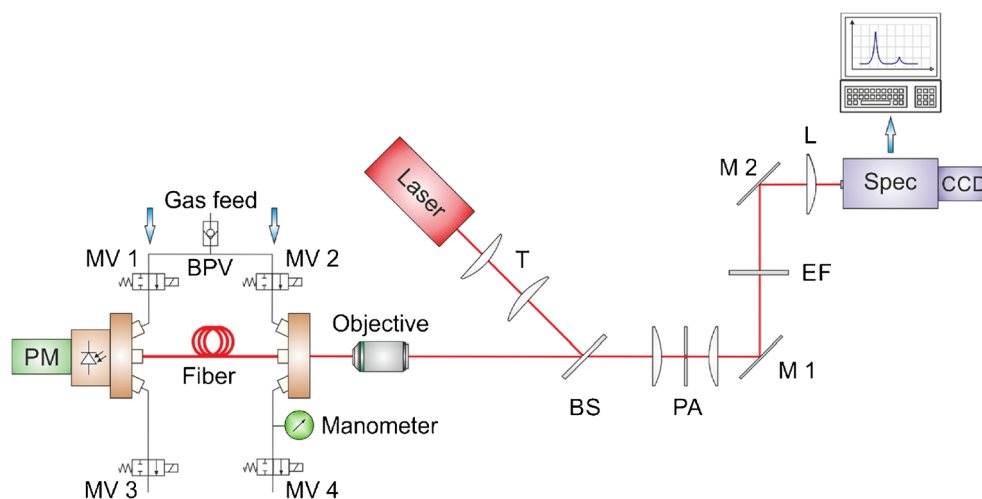
## Materials and methods

### FERS setup for Raman gas analysis

Raman spectroscopy is a highly selective technique which offers simultaneous detection and quantification of multiple compounds. Since light scattering in gases is a very weak process (Raman scattering cross section of most gases are in the range of  $10^{-32}$  cm<sup>2</sup> [48]), enhancement techniques are necessary to reach the goal of low detection limits (LOD) in the parts per million (ppm) range. As the Raman intensity scales linearly with the laser intensity and the number of interacting molecules [6], one approach to enhance signals is to increase the length of interaction between sample and highly intense laser light. This can be achieved using an optical waveguide, confining both, laser light and sample gas, within

its hollow core. Hollow core photonic crystal fibers (HC-PCF) are excellently suited for this purpose, guiding light within a broad spectral window and featuring a hollow core which can act as sample container. The optical design of the fiber-based Raman sensor is schematically illustrated in Fig. 2. The laser beam from a diode-pumped solid-state laser with a maximal output power of 250 mW at 640 nm (Lasos) is reflected by a dichroic beamsplitter (BS) into an objective (Olympus), where it is focused in a HC-PCF with a center wavelength of  $\sim$  675 nm and a bandgap suitable for low-attenuation guiding of Raman signals up to 3500 cm<sup>-1</sup>. The gases enter the HC-PCF via custom-made fiber adapters, which are installed at each end of the fiber. The adapters allow Raman light detection through optical windows. The sample gas can be fed into the fiber using magnetic valves. The fiber can be evacuated using a pump at the exhaust side. Light coupling into the fiber is achieved by a precisely controlled stage (nm-scale resolution). The scattered Raman signal is collected in backscattering geometry. A new assembly of two lenses and an adjustable pinhole in their confocal point (pinhole assembly, PA) was developed and used to suppress the glass background signal originating from the HC-PCF cladding [20]. Position and size of the pinhole are adjusted with micrometer precision in the image plane to block everything but the central part of the image, corresponding to the gas-filled hollow core of the fiber [57]. Compared with previous experimental setups [20], the crossed slit design of the pinhole enables fine adjustments to optimize the signal to noise ratio (SNR) with no need for pinhole exchange. The Raman signal is directed to a spectrometer (Spec, Acton SP2500, Princeton Instruments) equipped with a LN<sub>2</sub>-cooled CCD detector. Different gratings in the spectrometer allow overview measurements (grating with 300 lines/mm; corresponds to a resolution of 1.7 cm<sup>-1</sup>/pixel at 640 nm) and high-resolution measurements (grating with 1800 lines/mm; corresponds to a resolution of 0.4 cm<sup>-1</sup>/pixel at 640 nm). Gas feed, sensor and system control, as well as data acquisition and analysis were automated with LabVIEW.

**Fig. 2** Design of the HC-PCF-based Raman setup for gas analysis. PM, power meter; MV, magnetic valve; T, telescope; BS, beam splitter; PA, pinhole assembly; M, mirror; EF, edge filter; L, lens; Spec, spectrometer; CCD, liquid nitrogen cooled charged-coupled device



## Experimental design and measurement

To simulate common fuel gas compositions, a premixed certified gas mixture with the most prominent, typically occurring natural gas constituents (Table 1) and pure gases like methane, nitrogen, and carbon dioxide (purchased from Linde and Air Liquide) were used and precisely mixed by mass flow controllers (Brooks Instrument) with 1% reading accuracy. Gas mixing chambers provide homogeneous gas mixtures down to the ppb range. Before each individual measurement, the fiber was automatically evacuated and flushed with the sample gas for several times to avoid cross-contamination. By using a pump, pressures of up to 6 bar were applied. All measurements were performed at ambient temperature of 22 °C. Integration times between 1 and 30 s were used for most of the measurements. For low concentration measurements of H<sub>2</sub>S, exposure times up to 600 s were used. The laser power coupled into the fiber was 55 mW. In order to detect the low-wavenumber signals from C2–C4 alkanes in low concentrations, it is necessary to minimize the silica background to avoid sensor saturation for accumulation times longer than 1 s. Consequently, the pinhole size was set to 18 μm which corresponds to 49% of the fiber core area in the image plane. This fraction was found to be the most useful,

comparing glass background with gas signal levels and considering SNR. For each gas component, the respective Raman peak was fitted using a Lorentz distribution and integrated after background correction, yielding a peak area *A*. The peak area was subsequently normalized to the respective acquisition time. The SNR was calculated from the signal amplitude (*I*<sub>gas</sub>), divided by the standard deviation of the noise ( $\sigma_{\text{noise}}$ ) [40]:

$$\text{SNR} = \frac{I_{\text{gas}}}{\sigma_{\text{noise}}} \quad (1)$$

The normalized peak area *A* as well as the SNR were used as process parameters for the measurements to quantify simulated fuel gas compositions.

## Results and discussion

### Comparison of fuel gases of different origins

Hydrocarbon Raman signals occur in two major regions, between 700 and 1550 cm<sup>-1</sup> and between 2600 and 3200 cm<sup>-1</sup>

**Table 1** Composition of the gas mixture according to the specifications of the distributor as well as spectroscopic information of the components [22, 49, 54, 55]

Component	Specified concentration (vol%)	Measurement uncertainty (vol%)	Vibrational assignment	Raman peak position (cm <sup>-1</sup> )
Methane, CH <sub>4</sub>	92.3	1.8	$\nu_1$	2917
			$\nu_2$	1535
			$\nu_3$	3020
			$2\nu_4$	2585
Ethane, C <sub>2</sub> H <sub>6</sub>	3.5	0.07	$\nu_1$	2954
			$2\nu_8$	2914
			$2\nu_6$	2747
Nitrogen, N <sub>2</sub>	2.0	0.04	$\nu_3$	993
			$\nu_1$	2331
			$\nu_3$	2903
Propane, C <sub>3</sub> H <sub>8</sub>	1.2	0.024	$\nu_{11}$	1451
			$\nu_7$	1155
			$\nu_8$	870
			Hot band	1410
Carbon dioxide, CO <sub>2</sub>	0.5	0.01	$\nu_1$	1388
			$2\nu_2$	1286
			Hot band	1270
iso-Butane, i-C <sub>4</sub> H <sub>10</sub>	0.2	0.004	$\nu_2$	2890
			$\nu_7$	800
n-Butane, n-C <sub>4</sub> H <sub>10</sub>	0.2	0.004	$\nu_3$	2880
			$\nu_9$	830
iso-Pentane, i-C <sub>5</sub> H <sub>12</sub>	0.05	0.001		762
n-Pentane, n-C <sub>5</sub> H <sub>12</sub>	0.05	0.001		839

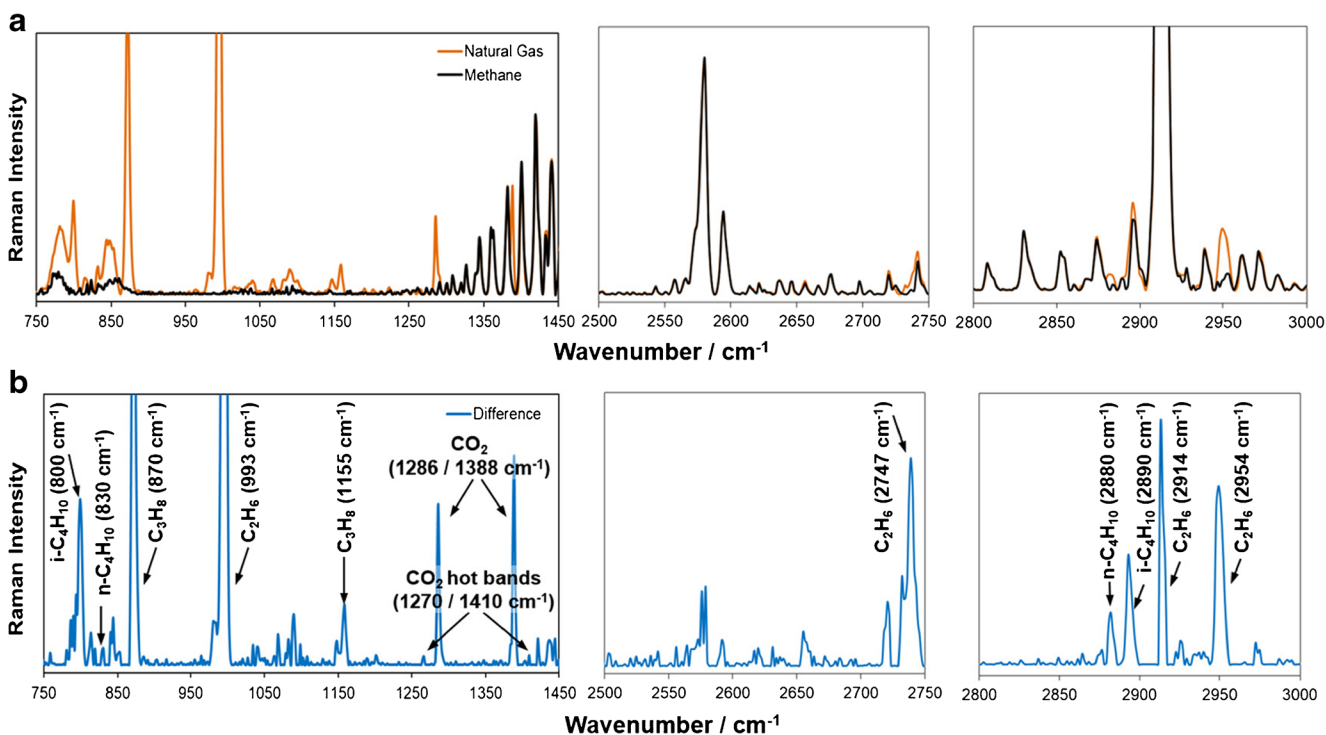
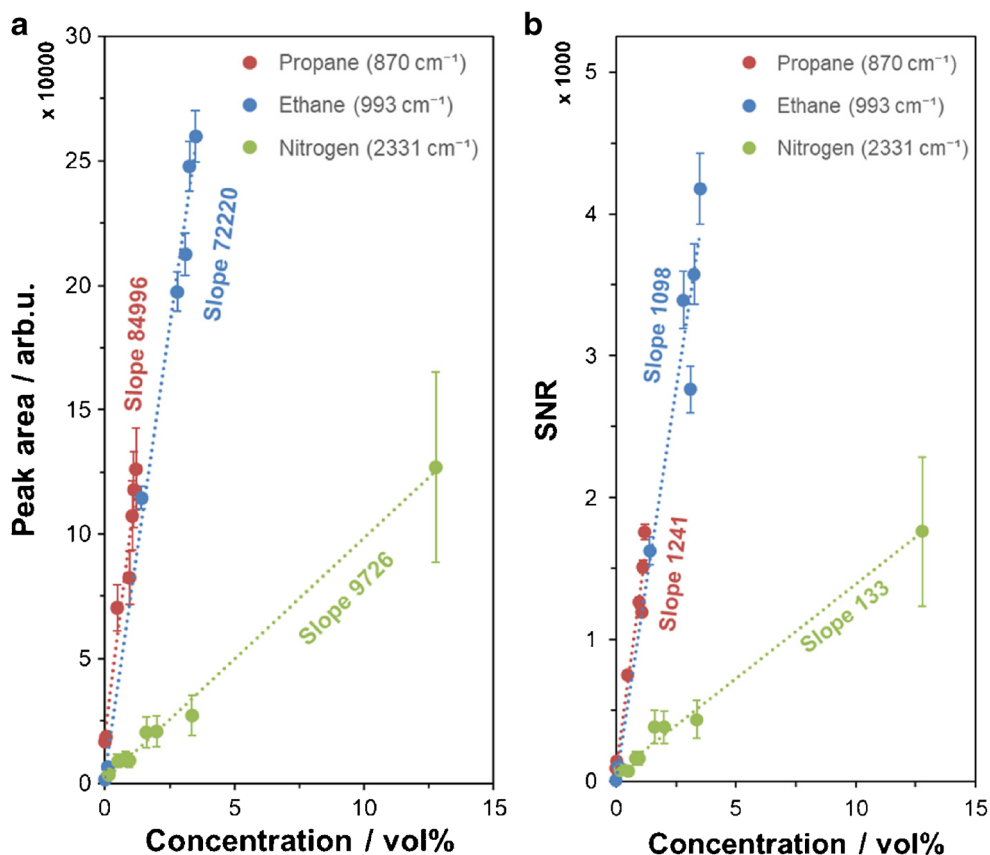


Fig. 3 Raman spectra of 5 bar **a** methane (black) and a typical natural gas mixture (orange) as well as their **b** difference spectrum (blue). Important gases and their spectral positions are assigned

Fig. 4 Linearity between **a** the normalized Raman peak area and the concentration and **b** the signal to noise ratio (SNR) and the concentration. The measured data were fitted linearly with coefficients of determination ( $R^2$ ) larger than 0.96. Error bars for nitrogen are partly smaller than the measurement points



**Table 2** Analytical parameters to characterize the sensor's performance regarding the peak area and SNR vs. the concentration. As described in the text, the detection limit was only determined via the SNR

Molecule	Slope		Relative standard deviation (%)		Coefficient of determination ( $R^2$ )		LOD (vol%)
	Peak area	SNR	Peak area	SNR	Peak area	SNR	
C <sub>2</sub> H <sub>6</sub> (993 cm <sup>-1</sup> )	72220	1098	4.0	6.7	0.99	0.96	0.003
C <sub>3</sub> H <sub>8</sub> (870 cm <sup>-1</sup> )	84996	1241	13.3	3.3	0.96	0.97	0.002

(Fig. 3). Both windows have their own advantages and limitations. In the lower wavenumber region, CH<sub>4</sub> shows only weak Raman signals and the signals of the other hydrocarbons are well separated. However, the HC-PCF generates increased background signals at 775 and 850 cm<sup>-1</sup>. As described above, the background was suppressed using a pinhole assembly. In the higher wavenumber region, the Raman signals of CH<sub>4</sub> and other hydrocarbons are stronger but produce spectrally overlapping peaks. Especially here, but also for the low-wavenumber region, interpretation and quantification can be facilitated in the subsequent data processing: Subtracting a spectrum of pure CH<sub>4</sub>, the main component of most fuel gases, a difference spectrum is obtained, showing the remaining components more clearly (Fig. 3b). Since all Raman signals of

the hydrocarbons and other components of natural gas are well known (Table 1), all remaining peaks could be assigned to the corresponding components. Ethane (C<sub>2</sub>H<sub>6</sub>), propane (C<sub>3</sub>H<sub>8</sub>), and iso- and n-butane (iso- and n-C<sub>4</sub>H<sub>10</sub>) show prominent Raman peaks in the range of the C-C stretching region below 1000 cm<sup>-1</sup>. The Raman signals for iso- and n-pentane (iso- and n-C<sub>5</sub>H<sub>12</sub>) are difficult to trace, since they overlap with the silica background from the HC-PCF. The Raman spectrum of carbon dioxide (CO<sub>2</sub>) is dominated by the Fermi resonance pair observed at 1286 and 1388 cm<sup>-1</sup> together with their hot band at 1270 and 1410 cm<sup>-1</sup>. The region near 3000 cm<sup>-1</sup> shows the C-H stretching fundamentals of the hydrocarbons. The Raman signal for C<sub>3</sub>H<sub>8</sub> at 2903 cm<sup>-1</sup> is not visible, due to interferences with ro-vibrational bands of the strong CH<sub>4</sub> signal at 2917 cm<sup>-1</sup>. For further measurements,

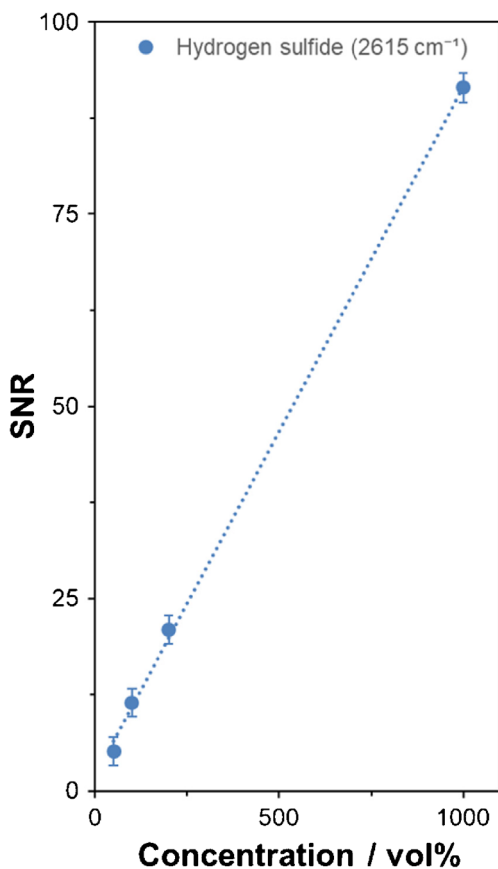


**Fig. 5** SNR of the H<sub>2</sub>S Raman peak at 2615 cm<sup>-1</sup> for different concentrations of H<sub>2</sub>S in argon. All peak fits have a  $R^2 > 0.95$  and the linear fit has a  $R^2 > 0.99$

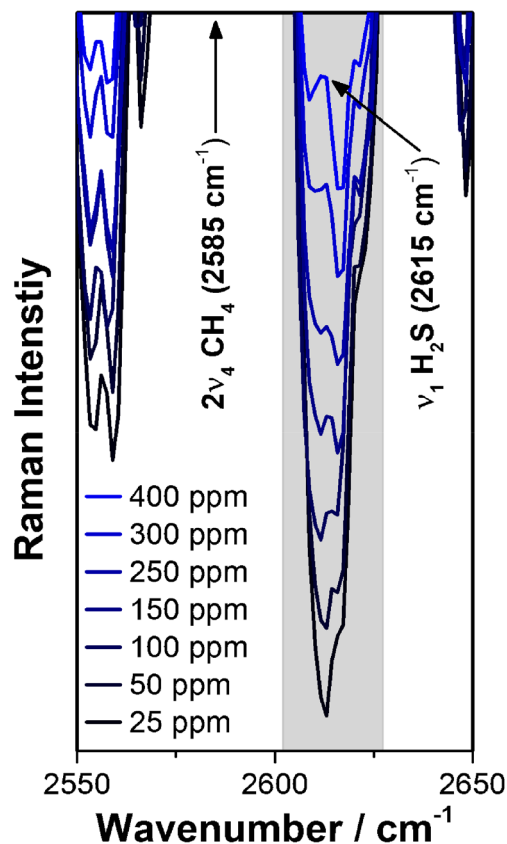


**Fig. 6** Raman spectra of a natural gas blend with varying concentrations of H<sub>2</sub>S from 400 ppm to 25 ppm. The Raman peaks of H<sub>2</sub>S and CH<sub>4</sub> are assigned

the lower wavenumber region was chosen, as it allows measuring prominent peaks of all main components with one single shot.

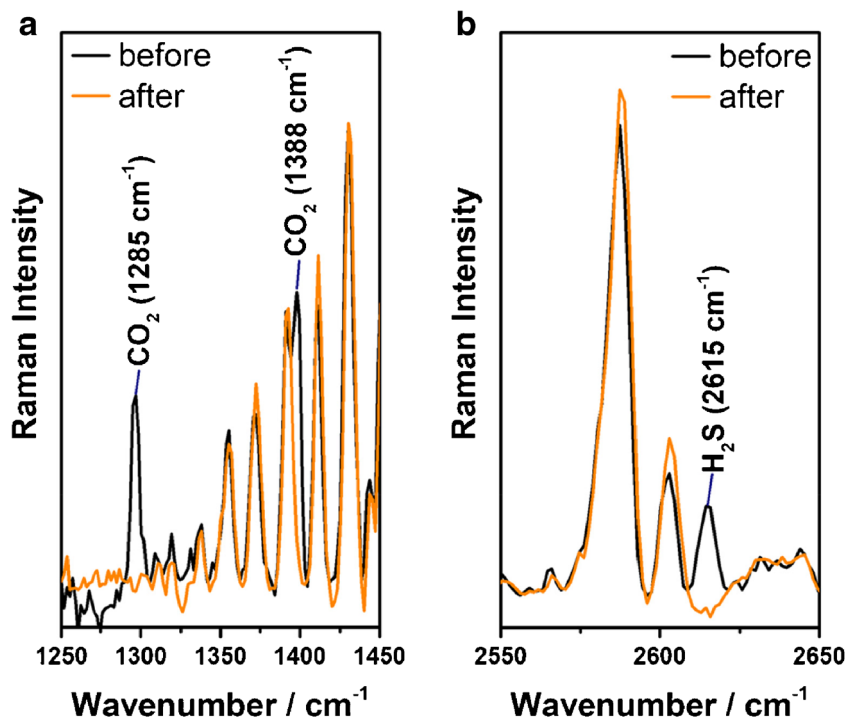
To simulate fuel gases from different origins, the primary natural gas mixture was mixed with pure gases like  $\text{CH}_4$ ,  $\text{N}_2$ , and  $\text{CO}_2$ . The mixtures (Table S1, see Electronic Supplementary Material, ESM) were chosen to mimic typical origins of different natural gases in Europe. H-natural gases (with a *high* calorific value), originate from the Commonwealth of Independent States (CIS) or the North Sea. L-natural gas is characterized by a low calorific value and originates from the Netherlands or Northern Germany. Biogas is produced by the anaerobic digestion of organic matter and consists mainly of a mixture of methane and carbon dioxide. Naturally, a content between 0 and 1 vol% hydrogen sulfide is possible [7]. To use biogas in the natural gas grid, the methane content must be increased, while other components must be removed or reduced [2], leading to bio-natural gas. Shale gas is a naturally formed gas that is found trapped within shale formations. As a fuel gas source, it is more important in the USA [16]. These various mixtures were analyzed using the developed FERS sensor. The completed measurements showed a very good linearity between the normalized Raman peak area as well as the signal to noise ratio (SNR) to the compound concentration (Fig. 4). Error bars represent the standard deviation between the measurements. The parameters to characterize the sensor's performance are summarized in Table 2. Coefficients of determination ( $R^2$ ) of more than 0.96 indicate a stable sensor performance. The steeper the slope, the more sensitive is the method. Especially for alkanes,

the developed FERS sensor is highly sensitive. The relative standard deviation (RSD = standard deviation/mean  $\times$  100%) was used to characterize the reproducibility. The RSD for methane is approx. 6%, for the higher hydrocarbons; it ranges from 5 to 15% (see Table 2). Reasons for the deviations could be slightly fluctuating environmental parameters as well as random variations such as noise. Additionally, post-processing introduces further errors. Using the SNR, the limit of detection for the minor components could be determined: LODs between 0.002 vol% for iso- $\text{C}_4\text{H}_{10}$  and  $\text{C}_3\text{H}_8$  as well as 0.003 vol% for  $\text{C}_2\text{H}_6$  were obtained. Due to the characteristic peaks for the individual molecules in the lower wave number range, the method based on FERS measurements is very specific especially for the lower concentrated C2+ components. The obtained results for the characterization of the different fuel gases are summarized in Table S1 (see Electronic Supplementary Material, ESM).

### Investigation of the $\text{H}_2\text{S}$ content in fuel gas and tracking of purification steps

Hydrogen sulfide ( $\text{H}_2\text{S}$ ) is a common minor component in natural gas deposits. Due to its high toxicity and corrosive nature, it is usually removed off shore before the natural gas is transmitted [21]. In biogas, the  $\text{H}_2\text{S}$  content can reach concentrations of up to 1 vol% [1]. Thus, the  $\text{H}_2\text{S}$  content must be reduced before the biogas can be fed into the natural gas grid. In addition to the desulfurization, a methane enrichment ( $\text{CH}_4$  content > 98%) and  $\text{CO}_2$  removal take place to ensure

**Fig. 7** Raman spectra of natural gas before (black) and after filtration (orange). The removal of **a** carbon dioxide ( $\text{CO}_2$  at 1286 and 1388  $\text{cm}^{-1}$ ) as well as **b** hydrogen sulfide ( $\text{H}_2\text{S}$  at 2615  $\text{cm}^{-1}$ ) is clearly visible. The filtration steps were done using soda lime and FerroSorp®



compatibility (Fig. 1). Sensors are needed to monitor this process and to ensure safety and usability of the processed biogas.

To prove the sensor system's suitability to measure H<sub>2</sub>S in low concentration ranges, a measurement series with different concentration values of H<sub>2</sub>S in argon was carried out, ranging from 1000 down to 50 ppm. The spectra were taken using 6 bar pressure and 60-s exposure time. The results show good linearity between concentrations and SNRs (Fig. 5). Using the SNR, it was possible to determine the limit of detection. A LOD of 33 ppm was calculated and shows the sensor's utility for detection of low H<sub>2</sub>S concentrations. Additionally, the detection of H<sub>2</sub>S in natural gas was tested. Here, concentrations of 400 to 50 ppm of H<sub>2</sub>S in natural gas were measured at 6 bar pressure and 600-s exposure time. The characteristic Raman peak of H<sub>2</sub>S could be differentiated from the surrounding ro-vibrational peaks of CH<sub>4</sub> for all concentrations with a SNR > 3 (Fig. 6).

Next, the FERS sensor was used to monitor purification steps via adsorptive filtration. Here, the separation of CO<sub>2</sub> and H<sub>2</sub>S from a biogas blend was performed using soda lime (mixture of calcium hydroxide (Ca(OH)<sub>2</sub>) and sodium hydroxide (NaOH)) and FerroSorp® (iron hydroxide (Fe(OH)<sub>3</sub>)). The biogas stream was monitored using FERS (Fig. 7). The Raman signal of H<sub>2</sub>S at 2615 cm<sup>-1</sup> was clearly visible besides the strong 2ν<sub>4</sub> band originating from CH<sub>4</sub> at 2585 cm<sup>-1</sup>. After the filtration step, neither CO<sub>2</sub> nor H<sub>2</sub>S was visible anymore in the Raman spectrum, confirming the successful purification by FERS measurements.

## Conclusion and outlook

A versatile gas sensor setup for online process monitoring of fuel gases was developed. Using a hollow core photonic crystal fiber for sensitivity enhancement, simultaneous detection of all important components including H<sub>2</sub>S, N<sub>2</sub>, CO<sub>2</sub>, and alkanes up to C<sub>4</sub> without cross sensitivity was feasible in just one single measurement. A recent study compared photonic-bandgap (PBG) to Kagomé-based HC-PCFs and concluded that PBG-PCFs strongly enhance the Raman gas signal but do not allow the measurement of gas components due to a strong background below 1700 cm<sup>-1</sup> [45]. However, we show here that the background signal generated from the glass material of a PBG-PCF can be reduced sufficiently using an adjustable pinhole assembly (Fig. 3). This feature allows the detection of minor components like butane or propane and limits of detection in the low ppm region (0.002 vol%). As a consequence, the presented LODs for the relevant higher hydrocarbons are better than the ones presented previously by a factor larger than 30 [45]. The FERS setup was also proven as H<sub>2</sub>S sensor (an LOD of 33 ppm was achieved). The LOD of H<sub>2</sub>S in CH<sub>4</sub> was 50 ppm and thus improved by a factor of approx. 2 compared with recently published Raman

spectroscopic results [23]. Excellent linearity of the obtained SNR as well as the normalized peak areas versus the component concentrations of typical fuel gas components (Fig. 4) demonstrates the stable performance of the FERS sensor. Additionally, the sensor system was successfully used to monitor the changes in the composition of a biogas blend during a purification process, eliminating H<sub>2</sub>S and CO<sub>2</sub> (Fig. 7).

Further investigations could focus on the determination of higher alkanes like pentanes and upwards (C<sub>5</sub>+). To achieve robust and reliable measurements, further steps have to be taken to stabilize the FERS system as well as to improve the post-processing of the data to achieve a highly reproducible quantification. The majority of industrial equipment operators judge the actual fuel gas composition a more relevant criterium than the Wobbe Index [35]. Current developments (in the European gas markets) will lead to frequent changes in local gas quality [35], emphasizing the need for comprehensive measurements onsite. This paper demonstrates the potential of FERS systems to serve this need as comprehensive sensors for industrial fuel gas analysis.

**Funding information** Funding was from the German Federal Ministry for Education and Research BMBF (03WKCV03E) and the Deutsche Forschungsgemeinschaft (DFG: CRC 1076 AquaDiva).

## Compliance with ethical standards

**Conflict of interest** The authors declare that they have no conflict of interest.

## References

1. Abatzoglou N, Boivin S. A review of biogas purification processes. *Biofuels Bioprod Biorefin.* 2009;3(1):42–71. <https://doi.org/10.1002/bbb.117>.
2. Al Mamun MR, Torii S. Enhancement of methane concentration by removing contaminants from biogas mixtures using combined method of absorption and adsorption. *Int J Chem Eng.* 2017:1–9. <https://doi.org/10.1155/2017/7906859>.
3. Berger R, Bothendorf E, Klinkert V, Meyer-Prescher B (2010) *Gasnetze der Zukunft: Studie zu den Auswirkungen der Biogaseinspeisung in das Erdgasnetz auf den Netzbetrieb und Endverbraucher.* Fraunhofer-Verlag.
4. Bogozí T, Popp J, Frosch T. Fiber-enhanced Raman multi-gas spectroscopy: what is the potential of its application to breath analysis? *Bioanalysis.* 2015;7(3):281–4. <https://doi.org/10.4155/bio.14.299>.
5. Bruckner M, Becker K, Popp J, Frosch T. Fiber array based hyperspectral Raman imaging for chemical selective analysis of malaria-infected red blood cells. *Anal Chim Acta.* 2015;894:76–84. <https://doi.org/10.1016/j.aca.2015.08.025>.
6. Demtröder W. *Laser Raman spectroscopy.* In: *Laser spectroscopy: basic concepts and instrumentation.* Berlin Heidelberg: Springer; 2003. p. 499–530. [https://doi.org/10.1007/978-3-662-05155-9\\_8](https://doi.org/10.1007/978-3-662-05155-9_8).
7. Deublein D, Steinhauser A. *Biogas from waste and renewable resources: an introduction.* Wiley; 2011.
8. Domes C, Domes R, Popp J, Pletz MW, Frosch T. Ultrasensitive detection of antiseptic antibiotics in aqueous media and human urine using deep UV resonance Raman spectroscopy. *Anal Chem.*



- 2017;89(18):9997–10003. <https://doi.org/10.1021/acs.analchem.7b02422>.
9. Domes R, Domes C, Albert CR, Bringmann G, Popp J, Frosch T. Vibrational spectroscopic characterization of arylisoquinolines by means of Raman spectroscopy and density functional theory calculations. *Phys Chem Chem Phys*. 2017;19(44):29918–26. <https://doi.org/10.1039/c7cp05415g>.
  10. Eichmann SC, Kiefer J, Benz J, Kempf T, Leipertz A, Seeger T. Determination of gas composition in a biogas plant using a Raman-based sensor system. *Meas Sci Technol*. 2014;25(7):075503.
  11. Faramawy S, Zaki T, Sakr AAE. Natural gas origin, composition, and processing: a review. *J Nat Gas Sci Eng*. 2016;34:34–54. <https://doi.org/10.1016/j.jngse.2016.06.030>.
  12. Friss AJ, Limbach CM, Yalin AP. Cavity-enhanced rotational Raman scattering in gases using a 20 mW near-infrared fiber laser. *Opt Lett*. 2016;41(14):3193–6. <https://doi.org/10.1364/OL.41.003193>.
  13. Frosch T, Popp J. Structural analysis of the antimalarial drug halofantrine by means of Raman spectroscopy and density functional theory calculations. *J Biomed Opt*. 2010;15(4):041516. <https://doi.org/10.1117/1.3432656>.
  14. Frosch T, Meyer T, Schmitt M, Popp J. Device for Raman difference spectroscopy. *Anal Chem*. 2007;79(16):6159–66. <https://doi.org/10.1021/ac070440+>.
  15. Frosch T, Chan KL, Wong HC, Cabral JT, Kazarian SG. Nondestructive three-dimensional analysis of layered polymer structures with chemical imaging. *Langmuir*. 2010;26(24):19027–32. <https://doi.org/10.1021/la103683h>.
  16. George DL, Bowles EB. Shale gas measurement and associated issues. *Pipeline Gas J*. 2011;238(7).
  17. Glindkamp A, Riechers D, Rehbock C, Hitzmann B, Scheper T, Reardon KF. Sensors in disposable bioreactors status and trends. *Adv Biochem Eng Biotechnol*. 2009;115:145–69. [https://doi.org/10.1007/10\\_2009\\_10](https://doi.org/10.1007/10_2009_10).
  18. Hanf S, Keiner R, Yan D, Popp J, Frosch T. Fiber-enhanced Raman multigas spectroscopy: a versatile tool for environmental gas sensing and breath analysis. *Anal Chem*. 2014;86(11):5278–85. <https://doi.org/10.1021/ac404162w>.
  19. Hanf S, Fischer S, Hartmann H, Keiner R, Trumbore S, Popp J, et al. Online investigation of respiratory quotients in *Pinus sylvestris* and *Picea abies* during drought and shading by means of cavity-enhanced Raman multi-gas spectrometry. *Analyst*. 2015;140(13):4473–81. <https://doi.org/10.1039/c5an00402k>.
  20. Hanf S, Bogoziti T, Keiner R, Frosch T, Popp J. Fast and highly sensitive fiber-enhanced Raman spectroscopic monitoring of molecular H<sub>2</sub> and CH<sub>4</sub> for point-of-care diagnosis of malabsorption disorders in exhaled human breath. *Anal Chem*. 2015;87(2):982–8. <https://doi.org/10.1021/ac503450y>.
  21. Hansen SB, Berg RW, Stenby EH. High-pressure measuring cell for Raman spectroscopic studies of natural gas. *Appl Spectrosc*. 2001;55(1):55–60. <https://doi.org/10.1366/0003702011951434>.
  22. Herzberg G. Infrared and Raman spectra of polyatomic molecules. New York: D. Van Nostrand Company; 1945.
  23. Hippler M. Cavity-enhanced Raman spectroscopy of natural gas with optical feedback cw-diode lasers. *Anal Chem*. 2015;87(15):7803–9. <https://doi.org/10.1021/acs.analchem.5b01462>.
  24. James TM, Rupp S, Telle HH. Trace gas and dynamic process monitoring by Raman spectroscopy in metal-coated hollow glass fibres. *Anal Methods*. 2015;7(6):2568–76. <https://doi.org/10.1039/c4ay02597k>.
  25. Jochum T, Michalzik B, Bachmann A, Popp J, Frosch T. Microbial respiration and natural attenuation of benzene contaminated soils investigated by cavity enhanced Raman multi-gas spectroscopy. *Analyst*. 2015;140(9):3143–9. <https://doi.org/10.1039/c5an00091b>.
  26. Jochum T, von Fischer JC, Trumbore S, Popp J, Frosch T. Multigas leakage correction in static environmental chambers using sulfur hexafluoride and Raman spectroscopy. *Anal Chem*. 2015;87(21):11137–42. <https://doi.org/10.1021/acs.analchem.5b03312>.
  27. Jochum T, Rahal L, Suckert RJ, Popp J, Frosch T. All-in-one: a versatile gas sensor based on fiber enhanced Raman spectroscopy for monitoring postharvest fruit conservation and ripening. *Analyst*. 2016;141(6):2023–9. <https://doi.org/10.1039/c5an02120k>.
  28. Jochum T, Fastnacht A, Trumbore SE, Popp J, Frosch T. Direct Raman spectroscopic measurements of biological nitrogen fixation under natural conditions: an analytical approach for studying nitrogenase activity. *Anal Chem*. 2017;89(2):1117–22. <https://doi.org/10.1021/acs.analchem.6b03101>.
  29. Keiner R, Herrmann M, Kusel K, Popp J, Frosch T. Rapid monitoring of intermediate states and mass balance of nitrogen during denitrification by means of cavity enhanced Raman multi-gas sensing. *Anal Chim Acta*. 2015;864:39–47. <https://doi.org/10.1016/j.aca.2015.02.007>.
  30. Keiner R, Gruselle MC, Michalzik B, Popp J, Frosch T. Raman spectroscopic investigation of <sup>13</sup>CO<sub>2</sub> labeling and leaf dark respiration of *Fagus sylvatica* L. (European beech). *Anal Bioanal Chem*. 2015;407(7):1813–7. <https://doi.org/10.1007/s00216-014-8446-8>.
  31. Kiefer J. Recent advances in the characterization of gaseous and liquid fuels by vibrational spectroscopy. *Energies*. 2015;8(4):3165–97.
  32. Kiefer J, Seeger T, Steuer S, Schorsch S, Weigl MC, Leipertz A. Design and characterization of a Raman-scattering-based sensor system for temporally resolved gas analysis and its application in a gas turbine power plant. *Meas Sci Technol*. 2008;19(8):085408.
  33. Knebl A, Yan D, Popp J, Frosch T. Fiber enhanced Raman gas spectroscopy. *TrAC Trends Anal Chem*. 2017;103:230–8. <https://doi.org/10.1016/j.trac.2017.12.001>.
  34. Knebl A, Domes R, Yan D, Popp J, Trumbore S, Frosch T. Fiber-enhanced Raman gas spectroscopy for <sup>18</sup>O–<sup>13</sup>C-labeling experiments. *Anal Chem*. 2019;91(12):7562–9. <https://doi.org/10.1021/acs.analchem.8b05684>.
  35. Leicher J, Giese A, Görner K, Werschy M, Krause H, Dörr H. Natural gas quality fluctuations – surveys and statistics on the situation in Germany. *Energy Procedia*. 2017;120:165–72. <https://doi.org/10.1016/j.egypro.2017.07.161>.
  36. Li XY, Xia YX, Huang JM, Zhan L. A Raman system for multi-gas-species analysis in power transformer. *Appl Phys B Lasers Opt*. 2008;93(2–3):665–9. <https://doi.org/10.1007/s00340-008-3170-8>.
  37. Long DA. The Raman effect: a unified treatment of the theory of Raman scattering by molecules. Wiley. 2002. <https://doi.org/10.1002/0470845767>.
  38. Markin AV, Markina NE, Goryacheva IY. Raman spectroscopy based analysis inside photonic-crystal fibers. *TrAC Trends Anal Chem*. 2017;88:185–97. <https://doi.org/10.1016/j.trac.2017.01.003>.
  39. Mazyan W, Ahmadi A, Ahmed H, Hoorfar M. Market and technology assessment of natural gas processing: a review. *J Nat Gas Sci Eng*. 2016;30:487–514. <https://doi.org/10.1016/j.jngse.2016.02.010>.
  40. McCreery RL. Raman spectroscopy for chemical analysis. Wiley; 2000.
  41. Petrov DV. Raman spectrum of methane in nitrogen, carbon dioxide, hydrogen, ethane, and propane environments. *Spectrochim Acta A Mol Biomol Spectrosc*. 2018;191:573–8. <https://doi.org/10.1016/j.saa.2017.10.058>.
  42. Qian Y, Sun SZ, Ju DH, Shan XX, Lu XC. Review of the state-of-the-art of biogas combustion mechanisms and applications in internal combustion engines. *Renew Sust Energ Rev*. 2017;69:50–8. <https://doi.org/10.1016/j.rser.2016.11.059>.
  43. Rupp S, Off A, Seitz-Moskaliuk H, James TM, Telle HH. Improving the detection limit in a capillary Raman system for in

- situ gas analysis by means of fluorescence reduction. *Sensors (Basel)*. 2015;15(9):23110–25. <https://doi.org/10.3390/s150923110>.
44. Salter R, Chu J, Hippler M. Cavity-enhanced Raman spectroscopy with optical feedback cw diode lasers for gas phase analysis and spectroscopy. *Analyst*. 2012;137(20):4669–76. <https://doi.org/10.1039/c2an35722d>.
45. Sandfort V, Trabold BM, Abdolvand A, Bolwien C, Russell PSJ, Wöllenstein J, et al. Monitoring the Wobbe Index of natural gas using Fiber-enhanced Raman spectroscopy. *Sensors*. 2017;17(12):2714. <https://doi.org/10.3390/s17122714>.
46. Schlüter S, Krischke F, Popovska-Leipertz N, Seeger T, Breuer G, Jelezov C, et al. Demonstration of a signal enhanced fast Raman sensor for multi-species gas analyses at a low pressure range for anesthesia monitoring. *J Raman Spectrosc*. 2015;46(8):708–15.
47. Schlüter S, Seeger T, Popovska-Leipertz N, Leipertz A (2016) Atemzyklusgenaues Anästhesiegas-Monitoring mit einer laserbasierten Raman-Sonde unter klinischen Bedingungen. *tm - Technisches Messen*, vol 83. <https://doi.org/10.1515/teme-2015-0055>.
48. Schrötter HW, Klöckner HW. Raman scattering cross sections in gases and liquids. In: Weber A, editor. *Raman spectroscopy of gases and liquids*. Berlin Heidelberg: Springer; 1979. p. 123–66. [https://doi.org/10.1007/978-3-642-81279-8\\_4](https://doi.org/10.1007/978-3-642-81279-8_4).
49. Shimanouchi T. Tables of molecular vibrational frequencies. Consolidated volume II. *J Phys Chem Ref Data*. 1977;6(3):993–1102. <https://doi.org/10.1063/1.555560>.
50. Sieburg A, Jochum T, Trumbore SE, Popp J, Frosch T. Onsite cavity enhanced Raman spectrometry for the investigation of gas exchange processes in the Earth's critical zone. *Analyst*. 2017;142(18):3360–9. <https://doi.org/10.1039/c7an01149k>.
51. Sieburg A, Schneider S, Yan D, Popp J, Frosch T. Monitoring of gas composition in a laboratory biogas plant using cavity enhanced Raman spectroscopy. *Analyst*. 2018;143:1358–66. <https://doi.org/10.1039/C7AN01689A>.
52. Speight JG. *Handbook of petroleum product analysis*, vol. 182. Wiley; 2015.
53. Ulbig P, Hoburg D. Determination of the calorific value of natural gas by different methods. *Thermochim Acta*. 2002;382(1):27–35. [https://doi.org/10.1016/S0040-6031\(01\)00732-8](https://doi.org/10.1016/S0040-6031(01)00732-8).
54. Van Helvoort K, Knippers W, Fantoni R, Stolte S. The Raman spectrum of ethane from 600 to 6500 cm<sup>-1</sup> Stokes shifts. *Chem Phys*. 1987;111(3):445–65. [https://doi.org/10.1016/0301-0104\(87\)85092-9](https://doi.org/10.1016/0301-0104(87)85092-9).
55. Weber A. *Raman spectroscopy of gases and liquids*. Berlin Heidelberg: Springer; 2012.
56. Yan D, Domes C, Domes R, Frosch T, Popp J, Pletz MW, et al. Fiber enhanced Raman spectroscopic analysis as a novel method for diagnosis and monitoring of diseases related to hyperbilirubinemia and hyperbilirubinemia. *Analyst*. 2016;141(21):6104–15. <https://doi.org/10.1039/c6an01670g>.
57. Yan D, Popp J, Frosch T. Analysis of fiber-enhanced Raman gas sensing based on Raman chemical imaging. *Anal Chem*. 2017;89(22):12269–75. <https://doi.org/10.1021/acs.analchem.7b03209>.
58. Yan D, Popp J, Pletz MW, Frosch T. Highly sensitive broadband Raman sensing of antibiotics in step-index hollow-core photonic crystal fibers. *ACS Photonics*. 2017;4(1):138–45. <https://doi.org/10.1021/acsphotonics.6b00688>.
59. Yan D, Popp J, Pletz MW, Frosch T. Fiber enhanced Raman sensing of levofloxacin by PCF bandgap-shifting into the visible range. *Anal Methods*. 2018;10(6):586–92. <https://doi.org/10.1039/c7ay02398g>.
60. Yan D, Frosch T, Kobelke J, Bierlich J, Popp J, Pletz MW, et al. Fiber-enhanced Raman sensing of cefuroxime in human urine. *Anal Chem*. 2018;90(22):13243–8. <https://doi.org/10.1021/acs.analchem.8b01355>.
61. Zachariah-Wolff JL, Egyedi TM, Hemmes K. From natural gas to hydrogen via the Wobbe index: the role of standardized gateways in sustainable infrastructure transitions. *Int J Hydrog Energy*. 2007;32(9):1235–45. <https://doi.org/10.1016/j.ijhydene.2006.07.024>.

**Publisher's note** Springer Nature remains neutral with regard to jurisdictional claims in published maps and institutional affiliations.